IET Microwaves, Antennas & Propagation

Research Article

IET Journals
The Institution of Engineering and Technology

Design strategy of concurrent multi-band Doherty power amplifier

ISSN 1751-8725
Received on 21st January 2015
Revised on 17th April 2015
Accepted on 2nd May 2015
doi: 10.1049/iet-map.2015.0033
www.ietdl.org

Robin Kalyan[1] ✉, *Karun Rawat*[2], *Shiban Kishan Koul*[1]

[1]*Centre for Applied Research in Electronics, Indian Institute of Technology, Delhi, Delhi, India*
[2]*Department of Electronics and Communication Engineering, Indian Institute of Technology, Roorkee, Roorkee, India*
✉ *E-mail: robin.kalyan@care.iitd.ac.in*

Abstract: This paper proposes design methodologies of concurrent multi-band Doherty power amplifiers (PAs) based on multi-band impedance inverting networks and multi-band phase offset lines (POLs). Design procedures for implementing such multi-band impedance inverting networks and multi-band POLs at arbitrary frequencies are presented here. For validating the design procedures, tri/quad-band Doherty PAs are designed, fabricated and tested using continuous wave (CW) and modulated signals in discrete mode and concurrent mode. The tri-band Doherty power amplifier (DPA) is implemented at 1600, 1900 and 2200 MHz. CW signal measurement of tri-band DPA shows an efficiency of 46%, 40% and 42%, respectively, around 6 dB output power back-off (OPBO). The quad-band DPA is implemented at 1600, 1960, 2140 and 2350 MHz. Measured results using CW signal shows an efficiency of 40%, 37%, 30% and 31%, respectively, around 6 dB OPBO.

1 Introduction

Recent advances in wireless technologies require concurrent multi-band/multi-standard power amplifiers (PAs) to operate simultaneously on several communication standards such as wideband code division multiple access (WCDMA) and worldwide interoperability microwave access (WiMAX) etc. These standards use signals with large peak to average power ratio (PAPR) [1] resulting into PA operating in certain output power back-off (OPBO) with poor efficiency. Several techniques such as supply modulation, out-phasing, load modulation etc., have been proposed to improve efficiency at OPBO [1, 2]. Out of these, load modulation technique in Doherty power amplifier (DPA) is mostly accepted [2–7]. Therefore implementation of multi-band DPA along with linearisation using digital pre-distortion (DPD) [7, 8], can significantly achieve all milestones of energy efficiency, spectrum efficiency and linearity simultaneously.

So far, researchers have mainly focused on dual-band DPAs [8–12]. Saad *et al*. [9] utilised T and pi-type components to achieve dual-band DPA characteristics, whereas in [8], dual-band T-type and coupled-line components were used to achieve frequency dependent OPBO in the two bands. Rawat and Ghannouchi [10], utilised pi-type dual-band phase offset lines (POLs) for efficiency enhancement. Similarly, Chen *et al*. [11] used impedance tuning at inter-modulation frequencies and [12, 13] utilised uneven power division for performance enhancement in DPA.

Recently, few works have been reported on tri-band and/or quad-band DPAs [14, 15]. The major limitation of the work reported in [14] is its applicability to fixed frequency ratios. Moreover, the reported work in [14] is based on asymmetric devices (10 and 25 W), that results in higher cost and higher circuit complexity because of different topologies for matching and stabilising networks of main and auxiliary PAs. The work in [15] reported a tri-band DPA but it lacks systematic design strategy. Therefore, the main focus of this paper is to present systematic design strategies for tri/quad-band DPAs which can be implemented at arbitrary frequencies (correlated or uncorrelated) using symmetrical devices.

2 Design strategy of multi-band DPA architecture

The proposed architecture for multi-band DPA is shown in Fig. 1 which is designed to operate at 6 dB OPBO with main PA biased in class-AB operation and auxiliary PA biased in class-C operation. The architecture in Fig. 1 is obtained by replacing some components of conventional DPA with corresponding multi-band components. As explained in [10], the POL is an important component in DPA which prevents any current leakage from main path (I_M) towards the auxiliary PA circuitry. This is achieved by transforming output impedance of auxiliary PA (denoted as $R_{A,out}$ in Fig. 1) to open circuit (O.C.) with the help of multi-band POL (POL_{Aux}). This additional phase shift added into the auxiliary path is compensated at the output of the main PA using POL_{Main}. In this work, a combination of simple transmission lines POL [14] and coupled-line POL [16] is proposed with the design procedure and advantages. Besides the POL, the IIN is an important component in the DPA which provides high load to the main PA at OPBO. For efficiency improvement at 6 dB OPBO, this high load is typically twice the load presented to the main PA at saturation. This paper adopts two different techniques to realise multi-band IIN. In tri-band DPA, a multi-band pi-type structure is utilised to obtain a tri-band IIN which is basically an extension of dual-band IIN [17]. For quad-band DPA, coupled-lines are used to realise IIN and the advantage of using this structure over pi-type IIN is described in the corresponding section. To compensate for these IIN at the output of tri/quad-band DPAs, an additional phase compensation network (PCN_i) is used at the input as shown in Fig. 1. The tri/quad-band DPAs are realised to cover distinct frequency bands in the frequency range of 1500–2500 MHz; therefore some components, such as input power splitter, multi-section impedance transformer, input/output matching networks (IMN and OMN) are designed as broadband components.

3 Design methodology for multi-band DPA components

This section briefs the design procedure for each component of Fig. 1.

3.1 Design of main and auxiliary PA

The main and auxiliary PAs are designed using the model of 10 W Gallium nitride (GaN) high electron mobility transistor (HEMT)

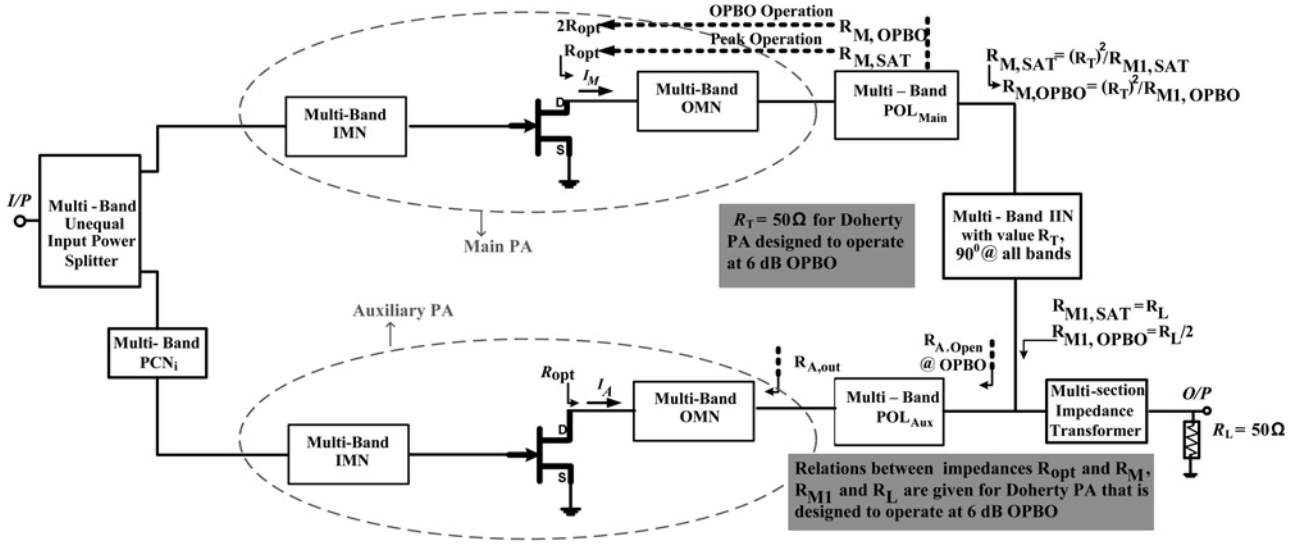

Fig. 1 *Proposed architecture for Tri/Quad-band DPA for 6-dB OPBO*

device from CREE. The Advanced Designed System is used for obtaining load pull results and the input impedance Z_{in} over the required frequency range as shown in Fig. 2*a*. Based on these simulated results, IMN and OMN are designed as described below.

3.1.1 Input matching: The operating frequencies of the multi-band DPAs are within 50% fractional bandwidth; therefore IMN and OMN are designed as broadband networks. In Fig. 2*a* the curve for Z_{in} shows a typical behaviour of series RLC modelled with $R_{in} = 7.5\ \Omega$, $L = 2.6$ nH and $C = 2.5$ pF. Matching network is then designed using unequally terminated filter design technique to absorb the reactive components (L and C) of the input model [18]. This will transform the required value of Z_{in} over the frequency range to a resistive input impedance of value kR_{in}, where, k is the transformation ratio of the unequally terminated band-pass filter prototype. An additional impedance transformer is then used to match the impedance kR_{in} to 50 Ω.

3.1.2 Output matching: One can see from the load pull simulation of the transistor in Fig. 2*a*, that the optimum output impedance point is clustered around $Z_{opt} = 25\ \Omega$ at saturation. Therefore, the optimum impedance point for the transistor must be clustered around $2Z_{opt} = 50\ \Omega$ at 6 dB OPBO. However, the multi-band IIN provides an impedance of 50 Ω at saturation and 100 Ω at OPBO because of load modulation. Hence, an OMN is required to transform 50 to 25 Ω at saturation and 100 to 50 Ω at OPBO; implying that the transformation ratio of the OMN remains same with the change in the load impedance. Thus the OMN is designed and tuned to provide this simultaneous matching condition at saturation and OPBO. It is worth mentioning here that POL_{Main} is added only to compensate for the phase of POL_{Aux} and does not affect matching at saturation.

3.1.3 Realisation of main and auxiliary PA: Since the multi-band DPAs are designed using symmetrical devices, therefore same schematic is used for both the main and auxiliary PAs. This schematic is shown in Fig. 2*b*, which includes biasing network, stability network, IMN and OMN. The ideal inductor in DC bias of Fig. 2*b* is replaced with a thin transmission line shorted with the bank of capacitors (of values from 1 pF–1 μF). The RC parallel network added in series to gate along with a shunt resistance of 150 Ω as shown in Fig. 2*b* are used to unconditionally stabilise the GaN HEMT device. All these values of components and dimensions for IMN and OMN are given in Fig. 2*b*.

3.2 Multi-band phase offset lines

In this section, a design strategy for multi-band POL is proposed which can be generalised to n number of arbitrary (correlated or uncorrelated) frequencies. The design procedure for multi-band POL requires S_{22} phase at the output of auxiliary PA biased in class-C mode. These values of S_{22} phase values are given in Table 1 for different frequencies of operation.

The proposed POL is a combination of simple transmission line POL [14] with transfer function given by (1) and N-section coupled-line POL [16] with transfer function given by (2)

$$S_{21,\mathrm{POL}} = \cos\theta_{\mathrm{POL}} - \mathrm{j}\sin\theta_{\mathrm{POL}} \tag{1}$$

where θ_{POL} is the electrical length of the transmission line POL [14] of Fig. 3*a*

$$S_{21,c} = \prod_{i=1}^{N}\left(\frac{\sqrt{\rho} - \mathrm{j}\tan\theta}{\sqrt{\rho} + \mathrm{j}\tan\theta}\right) \tag{2}$$

where ρ = Zoe/Zoo is the coupling co-efficient of coupled-line, θ is the electrical length of coupled-line. $Z_0 = \sqrt{Z_{0e}Z_{0o}}$ is the equivalent impedance of coupled-line, where, Z_{0e} and Z_{0o} are the characteristic impedances of the coupled line in even and odd-mode, respectively. It can be seen from (2) that N coupled-line sections have all-pass response and the non-linearity in phase response is controlled by ρ. Using this non-linearity of phase response, one can achieve better O.C. condition at arbitrary frequencies. To introduce non-linearity in phase response of simple POL [14], a section of simple POL shown as θ_c in Fig. 3*a* is replaced by N sections of coupled-lines. The proposed POL is also shown in Fig. 3*a*.

Based on (1) and (2), phase introduced by the proposed POL is given as

$$\varphi''_{i,POL} = -2n_i\theta_d + 2N\left(\arctan\left(-\left(\frac{\tan(n_i\theta)}{\sqrt{\rho}}\right)\right) - \arctan\left(\frac{\tan(n_i\theta)}{\sqrt{\rho}}\right)\right) \tag{3}$$

where $n_i = f_i/f_1$ and $i = 2, 3, 4, \ldots, n$ for frequencies $f_1, f_2, f_3, f_4, \ldots, f_n$, respectively. θ_d is the electrical length of simple delay line of the proposed POL as shown in Fig. 3*a*.

Based on (3), one can opt following procedure for calculating the design parameters of POL:

IET Microw. Antennas Propag., 2015, Vol. 9, Iss. 12, pp. 1313–1322

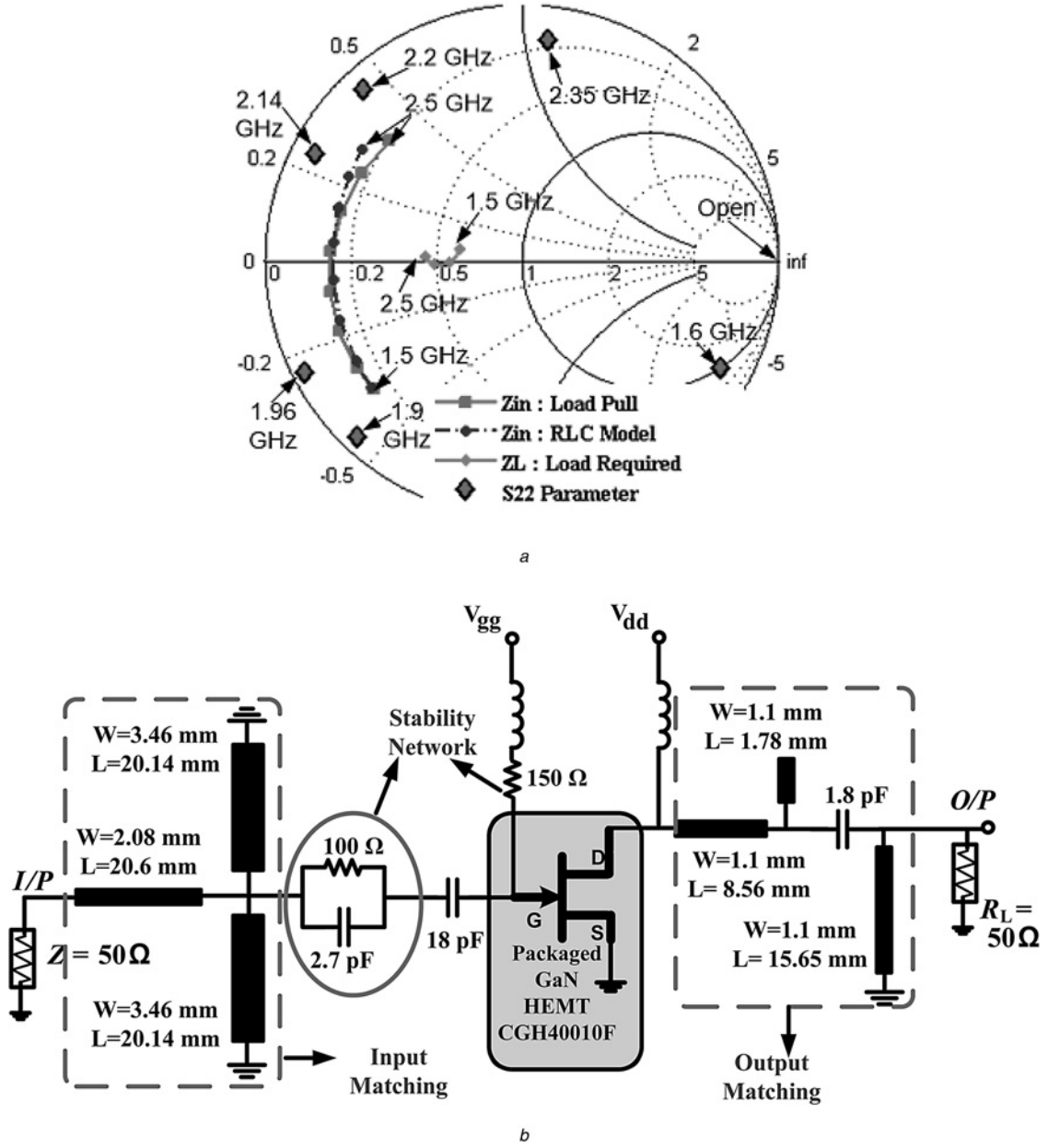

Fig. 2 *Design of proposed PA*

a Simulated source and load impedance for IMN and OMN and S_{22} parameter of auxiliary PA
b Schematic of designed main and auxiliary PA

Step 1: Initially set any physically realisable value of ρ (e.g. $\rho = 1.4$ is set in this case). This value will be optimised later for minimising the error in phase w.r.t. ideal O.C. condition.

Step 2: Choose a value of θ_d that solve two purposes: (a) to minimise the coupling among alternate lines in the coupled-line POLs; and (b) to help in the adjustment of final layout.

Table 1 Design requirements and design parameters of POLs for tri/quad-band DPAs

	Operating frequency, MHz	Values of S_{22} phase without offset lines	Calculated values of design parameters of coupled-line POL	Physical realised/optimised values of coupled-line POL	Simple transmission line POL
tri-band	1600	−28.3°	$L_d = 93.735$ mm $N = 2$	$L_d = 83.545$ mm $N = 2$	$L_{POL} = 218.35$ mm
DPA	1900	−133.16°	$W_{cs} = 1.07$ mm $S = 0.94$ mm	$W_{cs} = 1.09$ mm $S = 0.97$ mm	$W_{POL} = 107$ mm
	2200	132.5°	$L_{cs} = 32.24$ mm	$L_{cs} = 30.94$ mm	
quad-band	1600	−28.3°	$L_d = 188.09$ mm $N = 3$	$L_d = 183.45$ mm $N = 3$	$L_{POL} = 390.33$ mm
DPA	1960	−152.83°	$W_{cs} = 1.01$ mm	$W_{cs} = 1.38$ mm	$W_{POL} = 1.07$ mm
	2140	152.43°	$S = 0.198$ mm	$S = 0.26$ mm	
	2350	83.6°	$L_{cs} = 32.8$ mm	$L_{cs} = 31.86$ mm	

Where W_{cs} is width of coupled-Line section, S is spacing of coupled-Line section, L_{cs} is length of coupled-Line section and L_d is the length of simple delay line. L_{POL} and W_{POL} are the length and width of simple transmission line POL, respectively.

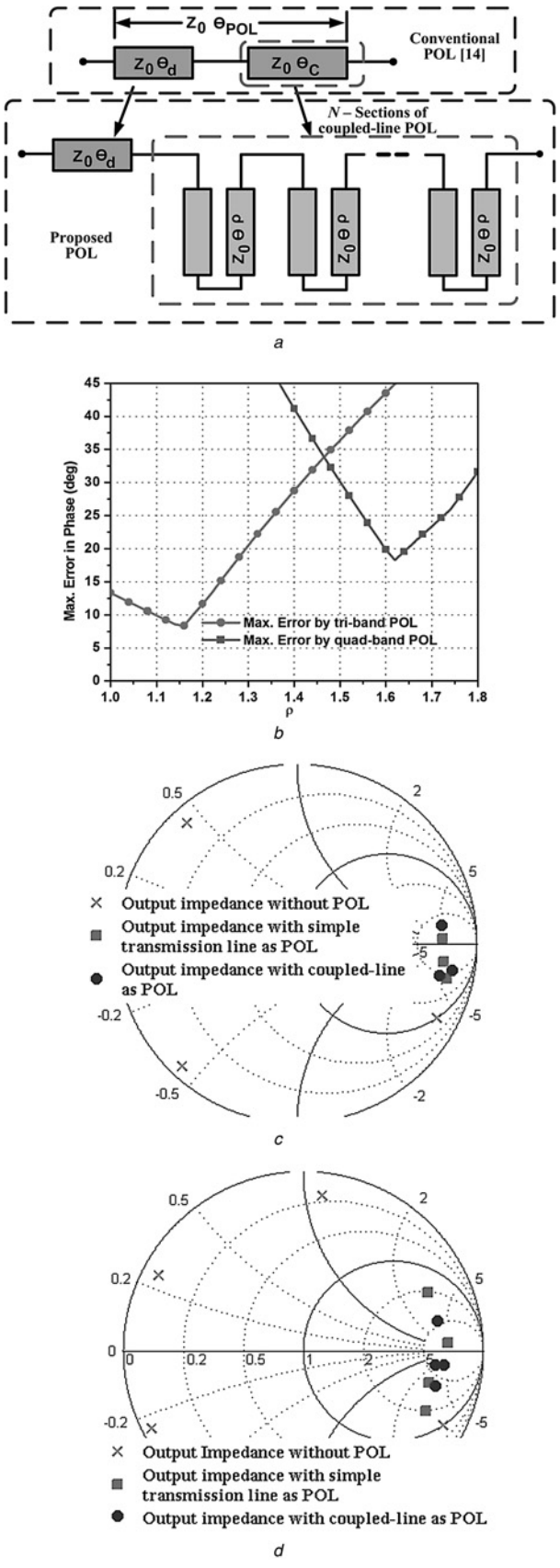

Fig. 3 *Design of proposed POL and its effect on output impedance of auxiliary PA*

a Schematic of conventional and proposed POL
b Maximum deviation (error) in phase w.r.t. O.C. condition against coupling coefficient (ρ)
c Output impedance of auxiliary PA at tri-band frequencies in class-C mode with and without offset lines
d Output impedance of auxiliary PA at quad-band frequencies in class-C mode with and without offset lines

Step 3: Using the values of ρ and θ_d as calculated in step 1–2, search an optimum value of coupled line electrical length θ for different values of N to minimise the error function of (4) to some limits (e.g. $\pm$30°) at all desired operating frequencies

$$\mathrm{ERR}_i = \varphi''_{i,\mathrm{POL}} + \varphi_i \tag{4}$$

where φ_i represents the initial phase of S_{22} obtained at the output of auxiliary PA at ith frequency.
Step 4: Based on the values of θ_d, N and θ as obtained in step 1 to 3, ρ is varied over a physically realisable range (1 to 1.8 in this case) to further minimise the error in (4). Fig. 3*b* shows this phase error minimisation w.r.t ρ of the coupled-lines for the given case of tri/quad-band DPA, from where, one can see that the optimum value of $\rho = 1.17$ provides minimum error in phase for tri-band operation and $\rho = 1.62$ provides minimum error in phase for quad-band operation.

Table 1 shows the calculated and optimised values for coupled-line POLs and simple transmission line POLs. Figs. 3*c* and *d* shows the effect of coupled line POL and simple transmission line POL at the output of tri/quad-band auxiliary PA. One can also see from Fig. 3*d* that a fair amount of improvement (more than 20°) is achieved in terms of O.C. condition by using proposed POL as compared with the simple transmission line POL.

3.3 Multi-band impedance inverting network

Referring to Fig. 1, the multi-band IIN is realised using a multi-band quarter-wave transmission line. The tri-band DPA utilises a tri-band IIN based on stub-loaded pi-type structure. This stub-loaded pi-type structure as shown in Fig. 4*a* is originally reported for dual-band operation [17]. In this paper, dual-band operation of pi-type structure is extended to tri-band operation as discussed below. The necessary conditions for pi-type structure of Fig. 4*a* to emulate quarter wave transformer characteristics of Z_0 characteristic impedance are given by [17]

$$Z_S \sin(\theta_S) = Z_0 \tag{5a}$$

$$B_S = \frac{1}{Z_S \tan(\theta_S)} \tag{5b}$$

where, Z_S and θ_S is respective characteristic impedance and electrical length of transmission line loaded with stub of susceptance jB_S as shown in Fig. 4*a*. To obtain quarter-wave response with perfect matching for three frequencies of operation, (5) should be satisfied at all three frequencies. This is not possible, however, if one allows some error in terms of realisation of perfect match (Z_0) at three desired frequencies as described next, then, an optimum solution can be obtained that will provide quarter wave line properties at three desired frequencies. If, n_1 and n_2 are the frequency ratios defined as $n_1 = f_2/f_1$ and $n_2 = f_3/f_1$, where f_1, f_2 and f_3 are first, second and third frequency of operation; then, at f_2 and f_3, one can write following relations

$$Z_S \sin(n_1 \theta_S) = Z_0 \tag{6a}$$

$$Z_S \sin(n_2 \theta_S) = Z_0 \tag{6b}$$

where, (5a) represents a similar condition at f_1. Using (5a) and (6b), one can express the following ratio

$$\frac{\sin(n_2 \theta_S)}{\sin(\theta_S)} = 1 \tag{7}$$

The value of θ_S can be obtained from (7) as given in [10]. This value of θ_S guarantees that (5a) and (6b) will be identical. Therefore for a given value of Z_0 (50 Ω in this case), a particular value of Z_S obtained using (5a) at f_1, will always satisfy (6b) at f_3, but gives some error in (6a) at f_2 in terms of Z_0. This error can be very high and hence deviates the effective characteristic impedance of tri-band IIN at f_2 far from Z_0. However, if slight error is also introduced in realising this effective characteristic impedance Z_0 at

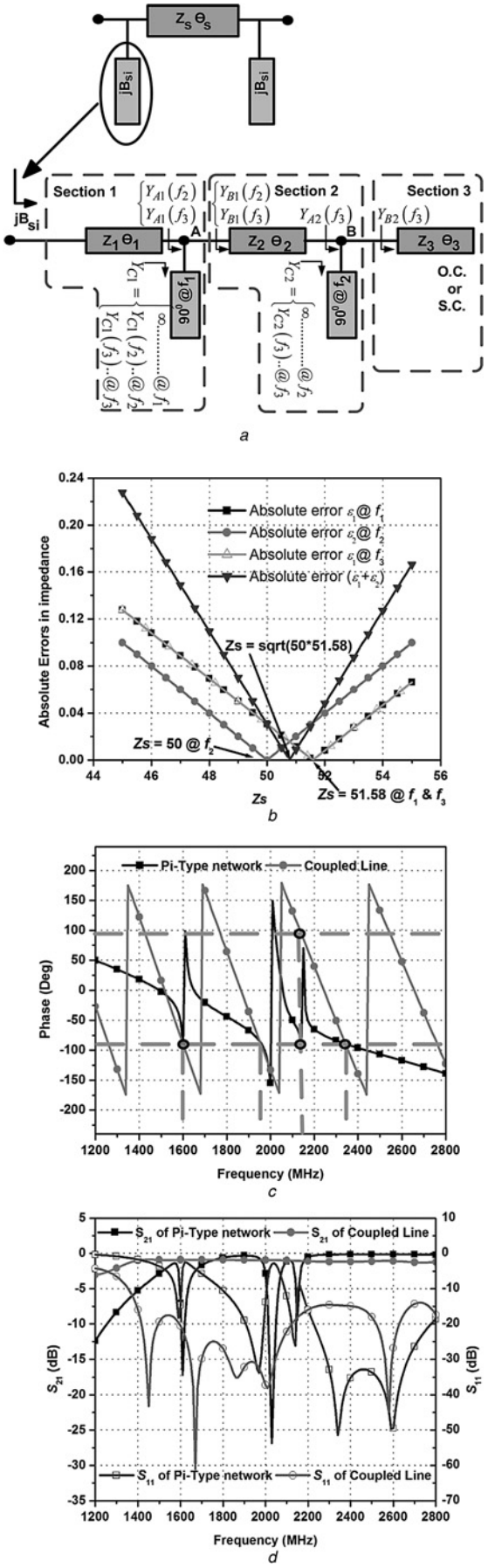

a

b

c

d

Fig. 4 *Design of multi-band IIN*

a Pi-type structure
b Impedance selection curves for tri-band pi-type network
c Comparison of phase response of pi-type inverter and coupled line inverter
d Comparison of magnitude response of pi-type inverter and coupled line inverter

f_1 and f_3, the error in Z_0 at f_2 can be minimised. In fact, the overall objective is to obtain desired Z_0 with minimum error equally distributed at each frequency f_1, f_2 and f_3. Therefore one can re-write (5a) for all the three frequencies of operation as

$$Z_S \sin(\theta_S) = Z_0 + \varepsilon_1 \tag{8a}$$

$$Z_S \sin(n_1\theta_S) = Z_0 + \varepsilon_2 \tag{8b}$$

$$Z_S \sin(n_2\theta_S) = Z_0 + \varepsilon_1 \tag{8c}$$

The value of Z_S is now obtained by minimising error ε_1 and ε_2 in (8). Fig. 4*b* shows the error in terms of realising Z_0 for different values of Z_S. From this figure, one can observe that the minima of the sum of errors ε_1 and ε_2 are obtained for the values of Z_S which is the geometric mean of the individual values of Z_S calculated from (8a) and (8b) for minimum and equal values of ε_1 and ε_2, respectively. This has also been established in literature [19] and this value of Z_S is given as

$$Z_S = \frac{Z_0}{\sqrt{(\sin(\theta_S)\sin(n_1\theta_S))}} \tag{9}$$

After calculating θ_S and Z_S from (7) and (9) respectively, susceptance values at different values are then calculated using (10)

$$B_{Si} = \frac{1}{Z_S \tan(n_{(i-1)}\theta_S)} \tag{10}$$

where $n_0 = 1$ and n_1 and n_2 as defined earlier for $i = 1, 2$ and 3 corresponds to the frequencies f_1, f_2 and f_3, respectively. These susceptance values are then realised using multi-section stub as shown in Fig. 4*a*. Referring to Fig. 4*a*, Section 1 realises B_{S1} with a short circuited transmission line of characteristic impedance Z_1 and electrical length θ_1 at f_1. Sections 2 and 3 will not affect realisation of B_{S1} at f_1 because of short at node A which is realised by 90° O.C. stub at f_1. After setting Section 1, the effect of Section 1 on susceptance B_{S2} at f_2 is de-embedded to obtain $Y_{B1}(f_2)$, such that when it terminates Section 1 at node A, the susceptance B_{S2} at f_2 is obtained at the input of Section 1. This $Y_{B1}(f_2)$ is then realised using Section 2 as shown in Fig. 4*a* in a similar fashion as Section 1 was designed. Similarly, by de-embedding the effect of Section 1 and Section 2 on B_{S3} at f_3, $Y_{B2}(f_3)$ is calculated, which is then realised by short or open stub in Section 3. The detailed methodology is given in [10].

For quad-band DPA, a pi-type network similar to tri-band pi-type network can also be used as IIN with a difference that the number of sections in multi-section stub will increase to four to realise four susceptances. The simulated response of such quad-band pi-type inverter is given in Figs. 4*c* and *d*. Fig. 4*c* shows that for quad-band pi-type IIN, the slope of simulated phase response with frequency is very high at 1600 and 2140 MHz. This is because of very high dispersive characteristic of stub-loaded structures [10]. A small error in hardware implementation of these sections can cause a significant error in results. Moreover, S_{21} response in Fig. 4*d* also shows high value of insertion loss at these frequencies which is perhaps because of more sections used in multi-section stubs. Therefore a coupled-line quad-band IIN is designed using the procedure similar to the design of coupled-line quad-band POL, except the required phases are ±90°. The simulated response of such coupled-line inverter are also given in Figs. 4*c* and *d*. Thus, from Figs. 4*c* and *d*, one can compare that the quad-band coupled-line inverter has a reasonable loss and good impedance matching in the desired frequency range, in addition to a phase shift of around 90° at desired frequency bands. Table 2 shows the design parameters of both the pi-type and coupled line based IIN.

3.4 Input power splitter

A single stage Wilkinson power divider (WPD) with unequal power division is used for power splitting in both tri/quad-band design [18]. Comparatively, more power is fed to the auxiliary PA to compensate

Table 2 Design parameters of tri/quad-band IIN

	Operating frequency, MHz	Calculated values of design parameters
tri-band	1600	$\theta_s = 75.79°$, $Z_s = 50.78\ \Omega$
DPA	1900	$B_{s1} = 4.9913$ mS, $B_{s2} = 0$ mS
	2200	$B_{s2} = -4.9917$ mS
quad-band	1600	$\theta_d = 694.4°@f_1$
	1960	$N = 4$
DPA	2140	$\theta = 101.714°@f_1$
	2350	$\rho = 1.58$

for its lower gain in the class-C bias operation. Besides WPD, the input splitting also includes an additional multi-band PCN_i to compensate for the phase introduced by IIN. Tri-band DPA uses pi-type structure, whereas, quad-band DPA uses coupled-line IIN as PCN_i as shown in Fig. 5. One can also use digital power splitting at the input [7] for achieving better phase compensation and improved performance.

4 Experiment and design consideration of tri-band and quad-band DPA

To validate the design strategy, tri/quad-band DPAs are designed and tested. The DPAs are realised for a 6 dB OPBO using symmetrical 10 W GaN HEMT devices (CGH40010F) from CREE. Main PA is biased in class-AB mode at $V_{ds} = 30$ V and $I_{ds} = 200$ mA whereas the auxiliary PA is biased in class-C mode. Both the DPAs are realised on RT4350B 20 mil substrate with a relative dielectric constant of 3.66. The photograph of fabricated DPAs are shown in Fig. 5.

5 Results and discussion

Both the DPAs are measured at discrete frequencies of operations as well as in concurrent mode. The measurements use continuous wave (CW) as well as complex modulated signals as input stimulus. The 5 MHz WCDMA and WiMAX signals with a PAPR of 7 dB are used for complex modulated signal measurements. The linearisation is done using DPD technique. The detailed description of results is given below.

5.1 Tri-band DPA measurement

5.1.1 CW measurement: The measured and corresponding simulated CW results for tri-band DPA are shown in Figs. 6*a*–*c*. The peak drain efficiency (DE) of 56.85, 58.72 and 58.57% are measured at 1600, 1900 and 2200 MHz, respectively. The corresponding power added efficiency (PAE) are 49, 51.26 and 43.43%. These measured values are taken at an output power level of 43.58, 43.83 and 42.36 dBm, respectively. At 6–7 dB OPBO, the measured DE are 46, 40 and 42% at 1600MHz, 1900MHz and

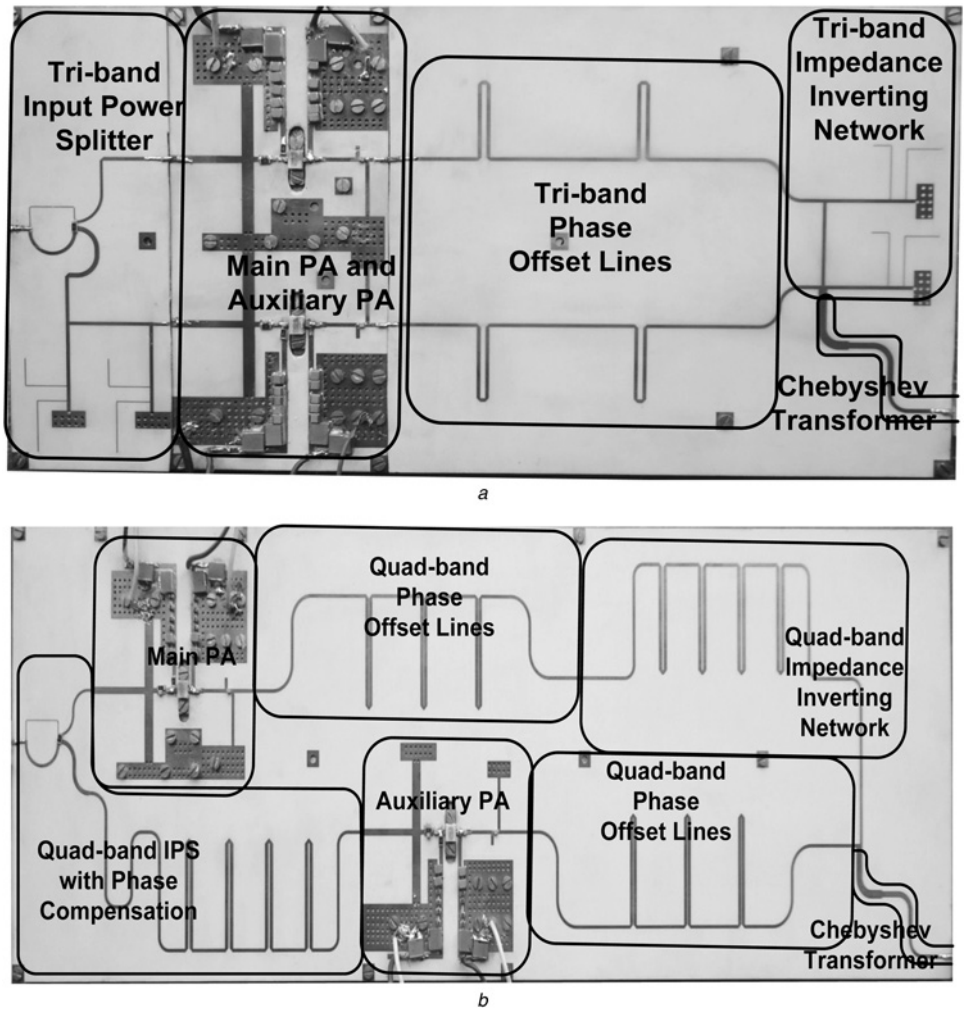

Fig. 5 *Photograph of fabricated DPA*

a Tri-band DPA
b Quad-band DPA

IET Microw. Antennas Propag., 2015, Vol. 9, Iss. 12, pp. 1313–1322

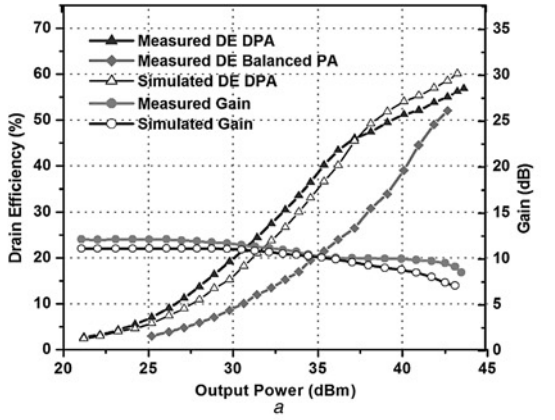

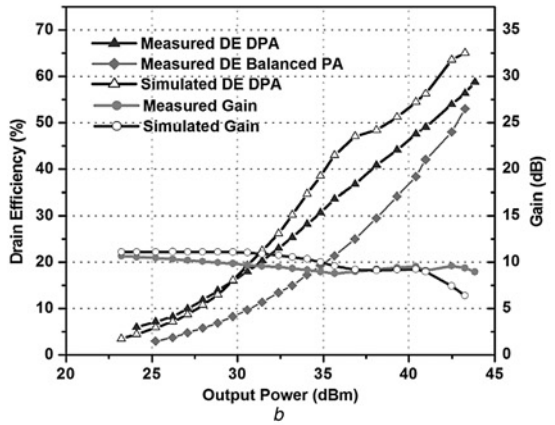

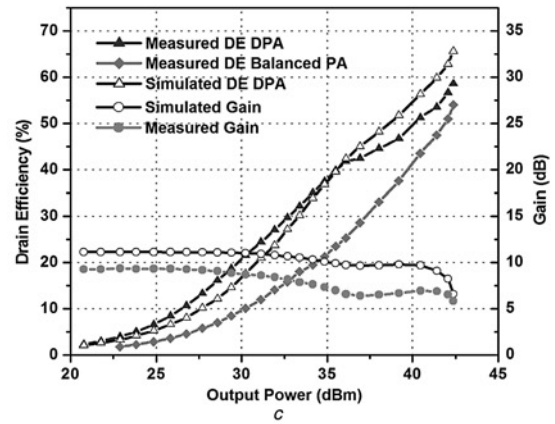

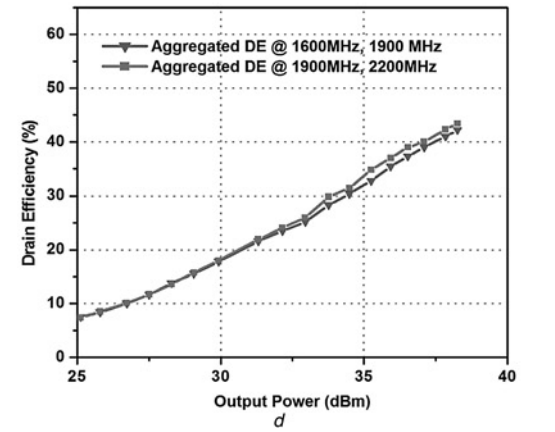

Fig. 6 *Performance of tri-band DPA*

a Using CW single tone signal at 1600 MHz
b Using CW single tone signal at 1900 MHz
c Using CW single tone signal at 2200 MHz
d Using modulated signals in concurrent operation

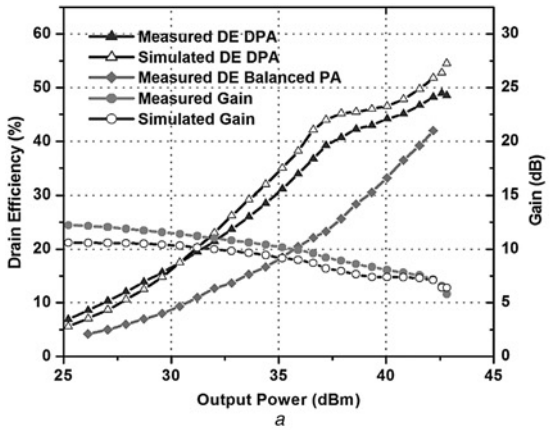

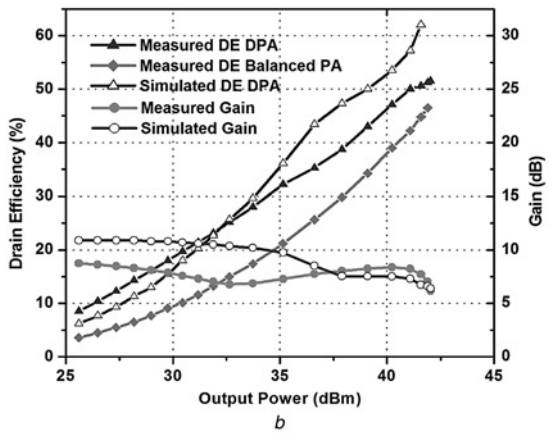

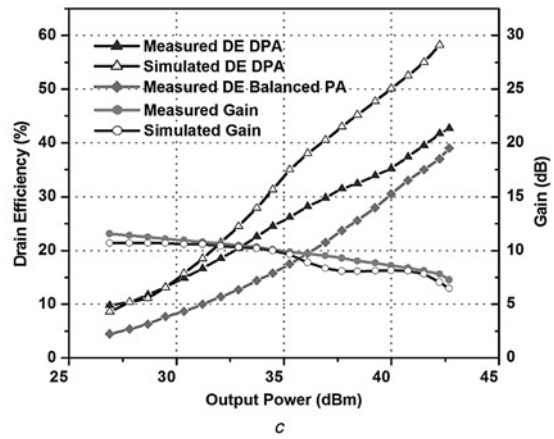

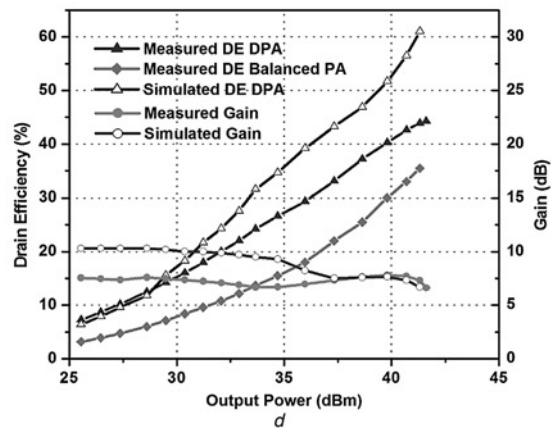

Fig. 7 *Performance of quad-band DPA*

a Using CW single tone signal at 1600 MHz
b Using CW single tone signal at 1960 MHz
c Using CW single tone signal at 2140 MHz
d Using CW single tone signal at 2350 MHz

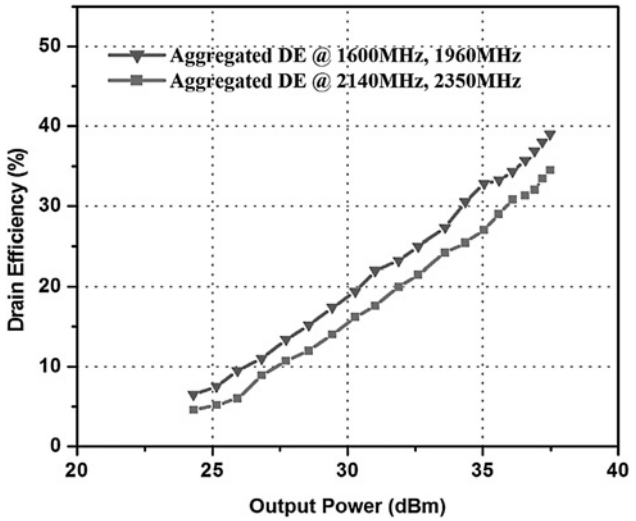

Fig. 8 *Measured aggregated DE of quad-band DPA in concurrent operation using modulated signals*

2200 MHz, respectively, and the OPBO PAE of 41.21, 34 and 32.7% are measured at these frequencies. These OPBOs corresponds to the output power of 37.2, 37.2 and 36.36 dBm, respectively. Figs. 6*a*–*c* shows that the PAE/gain decreases at higher operating frequencies and this is primarily because of poor input matching (as can be seen from Fig. 2*a*) and higher loss of passive circuits (IMN, OMN, POLs, IIN) at these frequencies.

In CW operation, DPA is also tested in balanced mode, where both the main and auxiliary PAs are biased in class-AB mode. Compared with balanced mode an efficiency improvement of 19.5, 11.5 and 15.3% at 1600, 1900 and 2200 MHz, respectively, is achieved at OPBO in Doherty operation.

5.1.2. Modulated measurement: Tri-band DPA is also tested with 5 MHz WCDMA and WiMAX signals in concurrent mode. However, because of the availability of only two vector signal generators, maximum concurrent operation was limited to two frequencies at a time. Accordingly, Fig. 6*d* shows two sets of concurrent measurements along with the measured aggregated DE. The aggregated DE is calculated as the ratio of net average RF output power (sum of average RF output power measured at different bands) to the net DC power consumed by the PA. From Fig. 6*d* concurrent aggregated DE at 1600 and 1900 MHz is measured as 40% at output power of 37.2 dBm whereas this value at 1900 and 2200 MHz is 40% at output power of 37.1 dBm.

5.2 Quad-band DPA measurement

5.2.1 CW measurement: The measured and corresponding simulated CW results for quad-band DPA are shown in Figs. 7*a*–*d*. The peak DE of 49, 51.2, 42.8 and 44.2% are measured at operating frequencies of 1600, 1960, 2140 and 2350 MHz, respectively. The corresponding measured PAE are 38, 41, 34.7 and 34.6% as shown in Figs. 7*a*–*d*. These figures show the respective DEs of 40, 37, 30 and 31% measured at OPBO and the corresponding PAE are 34.5, 31, 26.5 and 25.35%. The output power levels corresponding to this OPBO are 37.2, 37, 36.95 and 36.6 dBm, respectively.

One can see from Figs. 7*a*–*d* that as compared with balanced mode an efficiency improvement of 16, 9.4, 8.5 and 11% is achieved at OPBO in Doherty operation at 1600, 1960, 2140 and 2350 MHz, respectively.

It is worth mentioning that the efficiency at OPBO can further be improved by using asymmetric devices and biasing auxiliary PA in deep pinch-off to reduce soft turn-on effect [13, 14]. Moreover, the large POLs contributing to loss at the output can be removed if O.C. condition at the output of auxiliary PA is achieved by OMN as described in [20]. Moreover, a bare die device can also relax the requirements of O.C. condition.

5.2.2 Modulated measurement: The modulated measurement results are shown in Fig. 8, where, aggregated DE of 37.51% is achieved at an output power of 37 dBm while operating in concurrent mode at 1600 and 1960 MHz. The concurrent operation at 2140 and 2350 MHz results into measured aggregated DE of 32% at an output power of 36.61 dBm.

5.3 DPD measurement

DPD is performed using a conventional DPD scheme where a memory polynomial with 12 order non-linearity and three memory taps have been used for modelling the non-linearity of DPAs. For tri-band DPA, a 5 MHz WiMAX signal is used at carrier frequency of 1600 and 2200 MHz; whereas, a 5 MHz WCDMA signal is used at 1900 MHz. Similarly, for quad-band DPA, a 5 MHz WiMAX signal is used at carrier frequency of 1600 and 2140 MHz; whereas a 5 MHz WCDMA signal is used at 1960 and 2350 MHz. These linearisation results are shown in Figs. 9 and 10 for tri-band and quad-band DPAs, respectively. From Figs. 9 and 10, one can see that at all the frequencies of operation, the adjacent channel power ratio (ACPR) measured at an offset of 5 MHz is below −43 and −47 dBc for the tri-band and quad-band DPAs, respectively. Tables 3 and 4 reports the DPD performance of tri-band and quad-band DPAs, respectively, where, efficiency and output power at OPBO and ACPR with and without DPD are mentioned at each frequency.

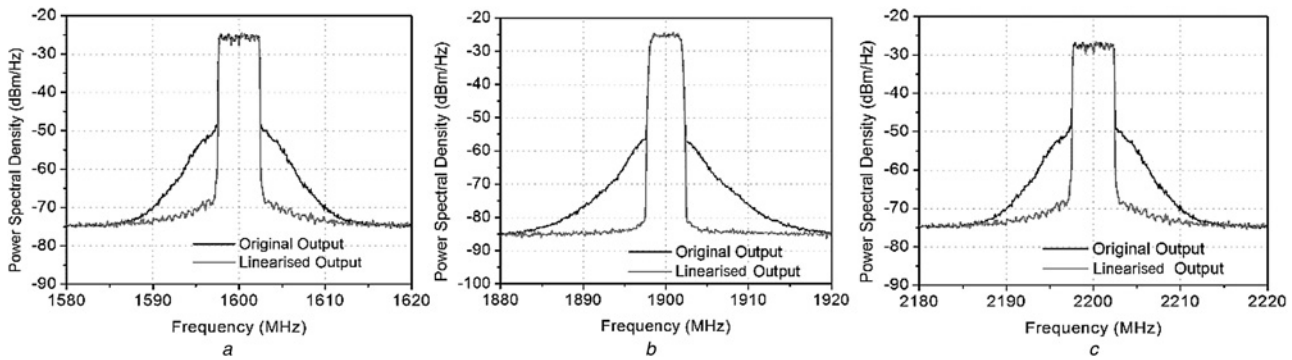

Fig. 9 *Output power spectral density of tri-band DPA with and without DPD*

a Using WiMAX signal at 1600 MHz
b Using WCDMA signal at 1900 MHz
c Using WiMAX signal at 2200 MHz

IET Microw. Antennas Propag., 2015, Vol. 9, Iss. 12, pp. 1313–1322

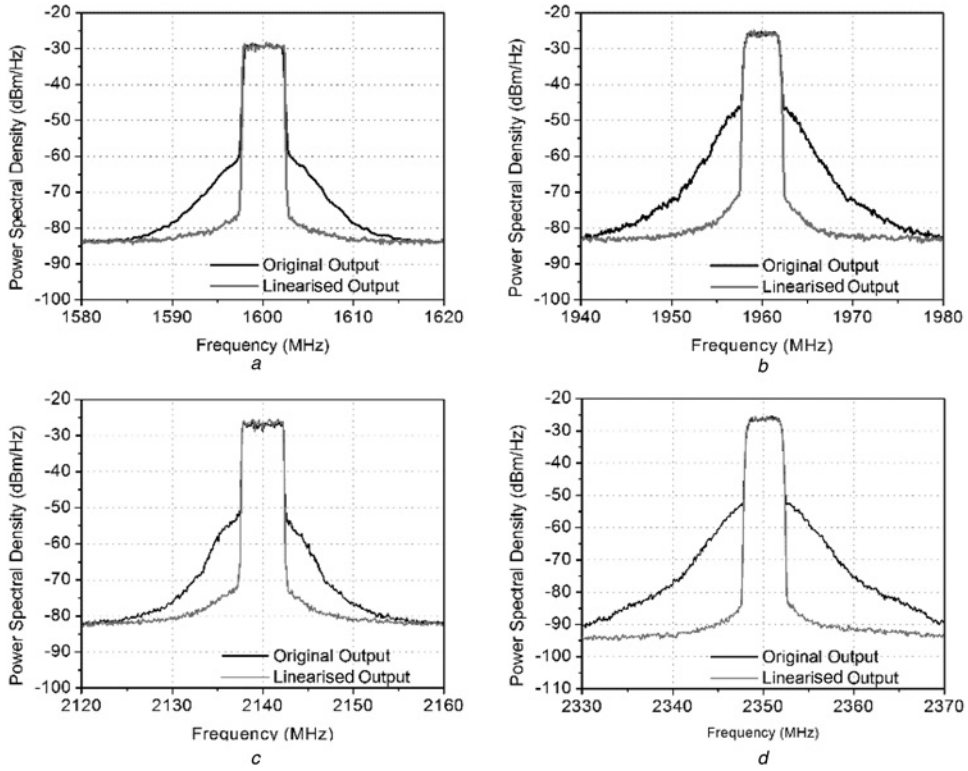

Fig. 10 *Output power spectral density of quad-band DPA with and without DPD*

a Using WiMAX signal at 1600 MHz
b Using WCDMA signal at 1960 MHz
c Using WiMAX signal at 2140 MHz
d Using WCDMA signal at 2350 MHz

Table 3 Summary of DPD linearisation of tri-band DPA

Signal type	Bandwidth, MHz	PAPR, dB	Frequency, MHz	Power @ 7 dB OPBO, dBm	Drain efficiency @ 7 dB OPBO, %	ACPR @ 5 MHz, dBc	
						DPD OFF	DPD ON
WiMAX	5	7	1600	36.2	40.1	−29.50	−44.58
WCDMA	5	7	1900	35.8	34	−38.72	−57.81
WiMAX	5	7	2200	35.51	38	−25.58	−42.58

Table 4 Summary of DPD linearisation of quad-band DPA

Signal type	Bandwidth, MHz	PAPR, dB	Frequency, MHz	Power @ 7 dB OPBO, dBm	Drain efficiency @ 7 dB OPBO, %	ACPR @ 5 MHz, dBc	
						DPD OFF	DPD ON
WiMAX	5	7	1600	32.41	23.8	−36.9	−51.1
WCDMA	5	7	1960	34.9	30.15	−28.78	−52.72
WiMAX	5	7	2140	34.68	26	−30.605	−47.49
WCDMA	5	7	2350	34.95	26.5	−34.38	−60.53

6 Conclusion

The proposed approach has been used for designing multi-band IIN and multi-band POLs. The foremost advantage of the proposed approach is its applicability to arbitrary frequency ratios. Moreover, this work emphasizes the design methodology of the multi-band DPA which are particularly useful when the operating frequencies are quite far-apart. To validate the design approach, tri/quad-band DPAs are implemented with symmetrical GaN HEMT devices. Such concurrent multi-band DPAs are useful for carrier aggregation as well as multi-standard operation in current wireless communication scenario.

7 Acknowledgments

Authors would like to acknowledge Department of Science and Technology, Government of India for financial support under project SB/S3/EECE/047/2014 and INSPIRE student fellowship. Authors are also thankful to Keysight Technologies for instrumental support.

8 References

1 Kennington, P.: 'RF and baseband techniques for software defined radio' (Artech House, Boston, 2005, 1st edn.), pp. 183–229

2 Raab, F.H., Asbeck, P., Cripps, S., *et al*.: 'Power amplifiers and transmitters for RF and microwave', *IEEE Trans. Microw. Theory Techn.*, 2002, **50**, (3), pp. 814–826
3 Doherty, W.H.: 'A new high efficiency power amplifier for modulated waves', *Proc. IRE*, 1936, **24**, (9), pp. 1163–1182
4 Bousnina, S.: 'Analysis and design of high-efficiency variable conduction angle Doherty power amplifier', *IET Microw. Antennas Propag.*, 2009, **3**, (3), pp. 416–425
5 Wu, D.Y.T., Boumaiza, S.: 'A modified Doherty configuration for broadband amplification using symmetrical devices', *IEEE Trans. Microw. Theory Tech.*, 2012, **60**, (10), pp. 3201–3213
6 Kim, B., Kim, J., Kim, I., Cha, J.: 'The Doherty power amplifier', *IEEE Microw. Mag.*, 2006, **7**, (5), pp. 42–50
7 Darraji, R., Ghannouchi, F.M.: 'Digital Doherty amplifier with enhanced efficiency and extended range', *IEEE Trans. Microw. Theory Tech.*, 2011, **59**, (11), pp. 2898–2909
8 Chen, W., Bassam, S.A., Li, X., *et al*.: 'Design and linearization of concurrent dual-band Doherty power amplifier with frequency-dependent power ranges', *IEEE Trans. Microw. Theory Tech.*, 2011, **59**, (10), pp. 2537–2546
9 Saad, P., Colantonio, P., Piazzon, L., *et al*.: 'Design of a concurrent dual-band 1.8–2.4-GHz GaN-HEMT Doherty power amplifier', *IEEE Trans. Microw. Theory Tech.*, 2012, **60**, (6), pp. 1840–1849
10 Rawat, K., Ghannouchi, F.M.: 'Design methodology for dual-band Doherty power amplifier with performance enhancement using dual-band offset lines', *IEEE Trans. Ind. Electron.*, 2012, **59**, (12), pp. 4831–4842
11 Chen, X., Chen, W., Ghannouchi, F.M., Feng, Z., Liu, Y.: 'Enhanced analysis and design method of concurrent dual-band power amplifiers with intermodulation impedance tuning', *IEEE Trans. Microw. Theory Tech.*, 2013, **61**, (12), pp. 4544–4558
12 Chen, W., Zhang, S., Liu, Y., Liu, Y., Ghannouchi, F.M.: 'A concurrent dual-band uneven Doherty power amplifier with frequency-dependent input power division', *IEEE Trans. Circuits Syst. I Reg. Pap.*, 2014, **61**, (2), pp. 552–561
13 Kim, J., Cha, J., Kim, I., Kim, B.: 'Optimum operation of asymmetrical -cells-based linear Doherty power amplifiers–uneven power drive and power matching', *IEEE Trans. Microw. Theory Tech.*, 2005, **53**, (5), pp. 1802–1809
14 Nghiem, X.A., Guan, J., Hone, T., Negra, R.: 'Design of concurrent multiband power amplifiers for wireless applications', *IEEE Trans. Microw. Theory Tech.*, 2013, **61**, (12), pp. 4559–4568
15 Rawat, K., Gowrish, B., Ajmera, G., *et al*.: 'Design strategy for tri-band Doherty power amplifier'. Proc. 15th Wireless and Microwave Technology Conf. (WAMICON), Tampa, Florida, June 2014, pp. 1–3
16 Rawat, K., Rawat, M., Hashmi, M.S., Falcone, F., Ghannouchi, F.M.: 'Dual-band phase offset line with required transmission phases at two operational frequencies'. IEEE MTT-S Int. Microwave Symp. Digest, Montreal, Canada, June 2012, pp. 1–3
17 Rawat, K., Ghannouchi, F.M.: 'Dual-band matching technique based on dual-characteristic impedance transformers for dual-band power amplifiers design', *IET Microw. Antennas Propag.*, 2011, **5**, (14), pp. 1720–1729
18 Gowrish, B., Rawat, K., Basu, A., Koul, S.K.: 'Broad-band matching network using band-pass filter with device parasitic absorption'. Proc. 82nd Automatic RF Techniques Group (ARFTG) Microwave Measurement Conf., Columbus, Ohio, November 2013, pp. 1–4
19 Piazzon, L., Saad, P., Colantonio, P., *et al*.: 'Design method for quasi-optimal multiband branch-line couplers', *Int. J. RF Microw. Comput. Aid. Eng.*, 2014, **24**, (1), pp. 117–129
20 Akbarpour, M., Helaoui, M., Ghannouchi, F.M.: 'A transformer-less load-modulated (TLLM) architecture for efficient wideband power amplifiers', *IEEE Trans. Microw. Theory Tech.*, 2012, **60**, (9), pp. 2863–2874